Atmos. Chem. Phys. Discuss., 13, 2913–2954, 2013
www.atmos-chem-phys-discuss.net/13/2913/2013/
doi:10.5194/acpd-13-2913-2013
© Author(s) 2013. CC Attribution 3.0 License.

Atmospheric Chemistry and Physics Discussions

This discussion paper is/has been under review for the journal Atmospheric Chemistry and Physics (ACP). Please refer to the corresponding final paper in ACP if available.

Radical mechanisms of methyl vinyl ketone oligomerization through aqueous phase OH-oxidation: on the paradoxical role of dissolved molecular oxygen

P. Renard[1], F. Siekmann[1], A. Gandolfo[1], J. Socorro[1], G. Salque[3], S. Ravier[1], E. Quivet[1], J.-L. Clément[2], M. Traikia[5], A.-M. Delort[5,6], D. Voisin[3], R. Thissen[4], and A. Monod[1]

[1]Aix-Marseille Université, CNRS, LCE FRE 3416, 13331 Marseille, France
[2]Aix-Marseille Université, CNRS, ICR UMR 7273, 13397 Marseille, France
[3]Université Joseph Fourier, Grenoble 1/CNRS-INSU, Laboratoire de Glaciologie et Géophysique de l'Environnement, 54 rue Molière, 38402 Saint-Martin-d'Hères, France
[4]Institut de Planétologie et d'Astrophysique de Grenoble (IPAG) UMR5274, UJF-Grenoble1/CNRS-INSU, Grenoble, 38041, France
[5]Clermont Université, Université Blaise Pascal, Institut de Chimie de Clermont-Ferrand, BP 10448, 63000 Clermont-Ferrand, France
[6]CNRS, UMR 6296, ICCF, BP 80026, 63171 Aubière, France

Received: 17 December 2012 – Accepted: 3 January 2013 – Published: 28 January 2013

Correspondence to: P. Renard (renard.pascal@yahoo.fr), A. Monod (anne.monod@univ-amu.fr)

Published by Copernicus Publications on behalf of the European Geosciences Union.

ACPD
13, 2913–2954, 2013

Abstract

It is now accepted that one of the important pathways of Secondary Organic Aerosol (SOA) formation occurs through aqueous phase chemistry in the atmosphere. However, the liquid phase chemical mechanisms leading to macromolecules are still not well understood. For α-dicarbonyl precursors, such as methylglyoxal and glyoxal, radical reactions through OH-oxidation produce oligomers, irreversibly and faster than accretion reactions. Methyl vinyl ketone (MVK) was chosen in the present study as it is an α, β-unsaturated carbonyl that can undergo such reaction pathways in the aqueous phase and forms even high molecular weight oligomers. We present here experiments on the aqueous phase OH-oxidation of MVK, performed under atmospheric relevant conditions. Using NMR and UV absorption spectroscopy, high and ultra-high resolution mass spectrometry, we show that the fast formation of oligomers up to 1800 Da is due to radical oligomerization of MVK, and 13 series of oligomers (out of a total of 26 series) are identified. The influence of atmospherically relevant parameters such as temperature, initial concentrations of MVK and dissolved oxygen are presented and discussed. In agreement with the experimental observations, we propose a chemical mechanism of OH-oxidation of MVK in the aqueous phase that proceeds via radical oligomerization of MVK on the olefin part of the molecule. This mechanism highlights the paradoxical role of dissolved O_2: while it inhibits oligomerization reactions, it contributes to produce oligomerization initiator radicals, which rapidly consume O_2, thus leading to the supremacy of oligomerization reactions after several minutes of reaction. These processes, together with the large ranges of initial concentrations investigated (60–656 µM of dissolved O_2 and 0.2–20 mM of MVK) show the fundamental role that O_2 likely plays in atmospheric organic aerosol.

ACPD

13, 2913–2954, 2013

1 Introduction

Although Secondary Organic Aerosol (SOA) represents a substantial part of organic aerosol, which affects air quality, climate and human health, the understanding of its formation pathways and its properties is still limited due to the complexity of the physicochemical processes involved. It is now accepted that one of the important pathways of SOA formation occurs through aqueous phase chemistry which is a favorable medium for the formation of oligomers (Hallquist et al., 2009; Carlton et al., 2009; Ervens et al., 2011). An oligomer is a molecule that consists of a few monomer units (roughly up to 30). Such aqueous phase chemistry is obviously relevant to clouds and fogs, but not limited to them, by far: it was shown that water can make up most of the aerosol mass, and in many cases largely exceeds the sum of all other particle species including organic matter (Tan et al., 2012; Liao and Seinfeld, 2005). This actually extends the relevance of aqueous phase processes from water vapor supersaturated regions of the atmosphere to high relative humidity regions, which represents a high fraction of the atmosphere. However, the aqueous phase chemical mechanisms leading to oligomers or macromolecules such as HULIS are still not well understood. Several accretion mechanisms such as aldol condensation, acetal formation or esterification have been tentatively proposed, but it was recently recognized that aqueous phase photochemistry plays a crucial role in oligomer development. For α-dicarbonyl precursors, such as methylglyoxal (Tan et al., 2012) and glyoxal (Lim et al., 2010), radical reactions through OH-oxidation produce oligomers, irreversibly and faster than accretion reactions.

Recent studies showed that aerosol water-soluble organic carbon (WSOC) is a complex mixture that contains thousands of organic compounds among which a majority is aliphatic to olefinic in nature, and indicate significant non-oxidative reaction pathways for the formation of high molecular weight WSOC components (Mazzoleni et al., 2012). Methyl vinyl ketone (MVK) was chosen for the present study as it is an α,β-unsaturated carbonyl that can possibly undergo such non-oxidative reaction pathways in the aqueous phase, as it was preliminarily shown by Liu et al. (2012).

ACPD
13, 2913–2954, 2013

The aim of the present study is to determine the radical mechanism involved in the oligomerization of MVK, and to identify the oligomers formed via this chemistry. The influence of atmospherically relevant parameters such as temperature, reactant initial concentrations and dissolved oxygen concentrations is studied.

2 Experimental

We used a photoreactor to simulate the aqueous phase photooxidation of MVK under atmospheric conditions. $HO^{\bullet}$ radicals were generated from H_2O_2 photolysis. In order to determine the reaction mechanism, we used a complete set of analytical strategies to identify the oligomers produced. Aqueous aliquots sampled at different photoreaction times were analyzed by mass spectrometry, UV absorbance spectroscopy and NMR. In order to test our radical mechanism for MVK oligomerization, its aqueous phase photooxidation was studied under various relevant conditions of temperature, MVK initial concentrations, and above all, dissolved oxygen concentrations.

2.1 Photoreactor

The photoreactor set-up we used is based on the one described by Liu et al. (2009, 2012) with some modifications. It is a 450 cm^3 Pyrex thermostated photoreactor. The arc light source (LSH 601, Lot Oriel) is equipped with a 1000 W xenon arc lamp (LSB 551, Lot Oriel). A glass filter (ASTM 892 AM 1.5 standard) was used to remove the UV irradiation below 300 nm, resulting in an irradiance spectrum comparable to that of the sun at sea level, for a 48.3° zenith angle, but more intense (less than an order of magnitude).

Compared to the set-up used by Liu et al. (2009, 2012), the photolysis rate constant of H_2O_2 increased by an order of magnitude due to the more powerful lamp used (Table 1). This resulted in higher $HO^{\bullet}$ concentrations using lower H_2O_2 initial

ACPD
13, 2913–2954, 2013

concentrations, and thus led to faster MVK degradation and kept artifacts due to H_2O_2 reactivity to a minimum.

A 50 mL gas space was left over the liquid level. The loss of aqueous MVK to the gas phase was insignificant, based on its Henry's Law constant (41 M atm^{-1} at 25 °C; Iraci et al., 1999) and on control experiments.

2.2 Experimental conditions

All experiments started with irradiation of UHQ water (18.2 Mohm cm, Millipore), then H_2O_2 (30 %, non-stabilized, Acros) was introduced, photolysed for 10 min until photostationary conditions were reached. MVK (99 %, Sigma Aldrich) was finally introduced at time noted 0 min. The experimental conditions (temperature, concentrations) were chosen in order to be representative of cloud droplets or deliquesced aerosol particles conditions.

2.2.1 Control experiments

To check that the observed products resulted from the aqueous phase OH-oxidation of MVK, two control experiments were conducted: (1) MVK (20 mM) + H_2O_2 (400 mM) under dark conditions, and (2) direct photolysis of MVK (20 mM). MVK was not significantly consumed either in presence of H_2O_2 in the dark (1) or under direct irradiation (2). Additionally, we performed (3) direct photolysis of H_2O_2 (400 mM) in absence of MVK, and the observed decrease of H_2O_2 concentrations allowed us to determine its photolysis rate constant J (see Table S1 in the Supplement). The duration of these three control experiments was 300 min, consistent with the reaction time of the actual MVK photooxidation experiments.

2.2.2 Initial concentrations of reactants

Tan et al. (2010) have shown the important impact of initial concentrations on oligomer formation for α-dicarbonyls. Our experiments were thus carried out with various

ACPD
13, 2913–2954, 2013

MVK initial concentrations i.e. 0.2 mM, 2 mM and 20 mM (corresponding to 9.6 to 960 mg C L^{-1}). These concentrations are representative of the total WSOC concentrations in atmospheric water from precipitation, cloud droplets to deliquesced aerosol particles (Decesari et al., 2005; Hennigan, et al., 2009).

We chose the ratio $[H_2O_2]_0/[MVK]_0$=20 to favor $HO^\bullet$ reaction toward MVK over its reaction with H_2O_2 (reaction R2, in Table S1 in the Supplement) by more than 90 %. Under these conditions, we estimated $HO^\bullet$ concentrations to approximately 5×10^{-14} M, which fall in the range of the estimated values for cloud droplets to deliquesced aerosol particles conditions by models (Herrmann et al., 2010; Ervens and Volkamer, 2010).

2.2.3 Temperature, pH and dissolved oxygen

Temperature, pH and dissolved oxygen concentrations were continuously monitored in the solution. Three relevant temperatures were tested, 5 °C, 9 °C and 25 °C. The pH of the unbuffered solution (monitored with a Consort C3020 multi-parameter analyzer) decreased from 6 to 3 within 90 min of photoreaction (Experiments A, B and C: $[MVK]_0$ = 20 mM, at 25 °C, 9 °C and 5 °C; Table 1).

At 25 °C, in experiments where dissolved oxygen concentrations were not constrained (Experiments A, B, C, E and F in Table 1), these concentrations were at Henry's law equilibrium with atmospheric O_2 in UHQ water. After H_2O_2 introduction (up to 400 µM in experiment A) the dissolved O_2 concentrations were supersaturated, due to H_2O_2 photooxidation (reactions R3 and R4 in Table S1 in the Supplement), and then they decreased down to nearly 0 during MVK photooxidation. Thus, for these experiments, O_2 was supersaturated when MVK was introduced (called "supersaturated initial O_2 concentrations" experiments in the following). Due to this high variability, and also because oxygen is known as a radical polymerization inhibitor (Odian, 2004), we investigated the influence of initial dissolved oxygen concentrations.

This is the reason why we also investigated "low initial O_2 concentrations" (experiments D) by bubbling a flow of argon in the solution before injecting MVK in order to evacuate as much O_2 as possible before the reaction started. Then the argon flow was

ACPD
13, 2913–2954, 2013

stopped in order to prevent MVK from evaporation, and the samples were collected using a syringe through a septum to avoid atmospheric O_2 entering the reactor.

2.3 Mass Spectrometry analyses of the solution

We used an ultra-high performance liquid chromatographic column coupled to a time of flight mass spectrometer equipped with a soft ionization electrospray source, noted UPLC-ESI-MS (Synapt-G2 HDMS, Waters). This instrument enabled us to evidence the oligomerization dependence on oxygen, and to follow the oligomerization kinetics. One of the experiments A (at 25 °C, Table 1) was performed using an ultra-high resolution mass spectrometer coupled to an electrospray ionization source, noted ESI-UHRMS (LTQ-Orbitrap-XL, Thermo).

2.3.1 UPLC-ESI-MS analyses

Aqueous samples (taken from the photoreactor) were analyzed for organics species using Quadrupole-Time-of-Flight Mass Spectrometry and Ion Mobility Spectrometry (Synapt G2 HDMS, Waters, MA, USA) combined with electrospray ion (ESI) source and coupled with an Acquity UPLC system (Waters). The mass spectrometer was used in its resolution mode, up to 18 000 FWHM (Full width at half maximum) at 400 Da and allowed the determination of elemental composition of some organic species, using the I-FIT software. The I-FIT isotope predictive filtering is a strategy to reduce the number of proposed elemental compositions using algorithms to estimate the number of carbon, oxygen or sulphur atoms in an unknown molecule based on the mass of the molecular ion and the relative intensity of the 1st and 2nd isotopes (Hobby, 2005).

The chromatographic separations were carried out on a HSS T3 UPLC column (Waters Acquity High Strength Silica T3, 2.1 × 100 mm, 1.8 µm) at 40 °C. The mobile phases consisted in (A) 0.1 % formic acid in water (Fluka, 98 %) and (B) Acetonitrile (CAN; Optima LC-MS, Fischer). The gradient elution was performed at a flow rate of 600 µL min^{-1}

ACPD
13, 2913–2954, 2013

using 5 to 95 % of B within 7 min and held at 95 % of B for 1.5 min. The sample injection volume was 10 µL.

The ESI source of this instrument contains two individual orthogonal sprays. One spray is for the column eluent, and the other one is for the internal standard called lock-mass. During each chromatographic run, leucine enkephalin (2 ng µL^{-1}, $C_{28}H_{37}N_5O_7$, MW 555.27, Waters Q-ToF product) was used for lock-mass correction to obtain accurate masses for each organic component eluting from the column. The lock-mass syringe pump was operated at 7 µL min^{-1}. A solution of sodium formate (CO_2HNa, Waters Q-ToF product) was infused daily in the ESI source to calibrate the instrument. Optimum ESI conditions were found using a 2.5 kV capillary voltage, 40 V sample cone voltage, 450 °C desolvation temperature, 120 °C source temperature, 20 L h^{-1} cone gas flow rate and 800 L h^{-1} desolvation gas flow rate.

Data were collected from 50 to 1800 Da in the positive and negative ionization modes. All products were detected as their protonated molecules ($[M+H]^+$) or sodium adducts ($[M+Na]^+$) in the positive mode, and their deprotonated molecules ($[M-H]^-$) in the negative mode.

For experiments A (Table 1), complementary analyses were performed using MS/MS fragmentation to confirm the structure of the products. MS/MS experiments (below 200 Da) were carried out with a trap collision energy ramp from 5 to 20 eV. Additionally, traveling wave ion mobility allowed us to separate ions which had the same elemental formula. The main parameters were the IMS Wave Velocity 650 m s^{-1} and the IMS Wave Height 40 V.

2.3.2 ESI-UHRMS analyses

One of the experiments A (at 25 °C, Table 1) was performed using an ultra-high resolution mass spectrometer coupled to an ESI source (LTQ-Orbitrap-XL, Thermo). Aqueous aliquots sampled from the photoreactor were diluted by a factor of 2 with ACN, and directly infused into the ESI at a 3 µL min^{-1} flow rate. Using a mixture (1:1) of ACN and aqueous samples helps the desolvation process in the ESI source, thereby ensuring

ACPD
13, 2913–2954, 2013

more stable operations. ACN was chosen against methanol as this latter was shown to occasionally induce esterification during the ionization (Bateman et al., 2008). Each sample was measured in the negative and positive ionization modes, with the following optimized settings: source voltage: 3.5 kV, capillary temperature: 275 °C, tube lens voltage: 50 V, in the positive mode, and source voltage: 3.7 kV, tube lens voltage: 90 V and same capillary temperature in the negative mode.

Transient acquisition time was set to 1s, which corresponds to a nominal resolution of 100 000 at 400 Da, and to observe individual peaks resolution (FWHM) typically better than 200 000 at 200 Da. Each spectrum was obtained by averaging 20 min of acquisition time, so as to increase the *S/N* ratio of the lower intensity peaks. Acquisition was performed over two overlapping mass ranges: 50–300 Da and 150–1500 Da. This method overcomes transfer limitations of very wide mass ranges in the ion optics which guide the molecular ions through the LTQ to the Orbitrap mass analyzer.

External mass calibration was made daily by infusing a calibration mixture (L-methionine-arginyl-phenylalanyl-alanine, caffeine, and ultramark: MSCAL 5-10EA Supelco) having peaks in the range 195 to 1921 Da. The obtained mass accuracy was as low as 2–5 ppm, and better for peaks with a relative intensity above 0.5 % (Makarov et al., 2006).

For our moderately complex mixture (~ 6000 peaks), containing only O, C, H, and Na, unambiguous elemental formula assignments were established below 350 Da within 1 mDa using a custom computer software (Attributor v1.05) developed by F. R. Orthous-Daunay (2011) and described in Danger et al. (2013). It is based on a suite of scripts that allow to evaluate the most probable attribution of a high resolution peak, based on its mass, the presence and relative intensity of isotopic peaks, as well as chemical rules (nitrogen rule, even electron ions, etc.) Using a Kendrick analysis (Hughey et al., 2001) based on the MVK pattern (i.e. C_4H_6O) found by Liu et al. (2012) and on the unambiguous attribution of most peaks below 350 Da, series of regularly spaced peaks were identified in the spectrum, and used to extend the formula attribution toward higher masses. This extension into Kendrick series was also checked against isotopic

ACPD
13, 2913–2954, 2013

patterns. Typical standard deviation of the Kendrick mass defect in any such identified series was lower than 0.5 mDa which ensures the proper attribution of all the members of a series, to within less than 1 mDa in the full mass range explored (i.e. 50–1500 Da).

2.4 Spectroscopic analyses of the solution

2.4.1 UV Spectroscopy

UV absorption spectroscopy (Agilent 8453) was used in a wavelength range from 190 to 400 nm to monitor MVK concentrations and chemical structure changes during the reaction. Diluted in water, MVK shows, like all α,β-unsaturated ketones (Yadav, 2012), an intense absorption band (K-band; $\pi \rightarrow \pi^*$ transition) at 211 nm (ε_{211} = 7692 $M^{-1}\,cm^{-1}$) and a weak absorption band (R-band; $n \rightarrow \pi^*$ transition) at 296 nm (ε_{296} = 30 $M^{-1}\,cm^{-1}$). Because the absorbance of H_2O_2 below 240 nm is intense (i.e. ε_{211} = 100 $M^{-1}\,cm^{-1}$), it was interfering with the $\pi \rightarrow \pi^*$ transition of MVK under our experimental conditions where $[H_2O_2]_0/[MVK]_0$=20. A volume of catalase from bovine liver (C 3155, Sigma Aldrich) was added to each sample to quench efficiently the H_2O_2 absorbance signal within a few minutes (Li and Schellhorn, 2007).

2.4.2 NMR spectroscopy

One of the experiments A was analyzed using NMR spectroscopy (Table 1). The instrument used was a Bruker Avance 500 MHz equipped with a 5 mm inverse-triple tuned (TXI) $^{1}H/^{13}C/^{15}N$ with z-gradient coil probe. For 1-D ^{1}H-Spectra, 128 scans were collected with an impulsion time of 7.5 µs, a relaxation delay of 5 s, an acquisition time of 4.67 s, a spectral window of 5000 Hz and 64 K data points zero-filled to 128 K before Fourier transformation with 0.3 Hz line broadening. For 2-D homonuclear (COSY and TOCSY) and heteronuclear ($^{1}H/^{13}C$ HSQC and HMBC) experiments were performed with quadrature phase detection in both dimensions, using state-TPPI or QF detection mode in the indirect one. For each 256 (homonuclear experiments) or

ACPD
13, 2913–2954, 2013

512 (heteronuclear experiments) increments in the indirect dimension, 2K data points were collected and 16 or 32 transients were accumulated in the direct dimension. ^{13}C decoupling (GARP) was performed during acquisition time for heteronuclear experiments. A $\pi/2$ shifted square sine-bell function was applied in the indirect dimension before Fourier transformation. Spectra were treated with Topspin version 2.0. All NMR spectra were recorded at 25 °C.

Aliquots of 540 µL of the aqueous solution sampled from the photoreactor (at 5, 10, 25, 70 and 90 min of reaction) was supplemented with 60 µL of a buffer containing 100 mM phosphate and 5 mM of sodium tetra deuterated trimethylsilyl propionate ($TSPd_4$, Eurisotop). $TSPd_4$ constituted a reference for chemical shifts (0 ppm) and quantification. Final volumes of 600 µL of prepared samples were put in 5 mm-diameter NMR tubes.

Additionally, an aliquot of 5 mL sampled at the end of the kinetic (90 min of reaction) was freeze-dried, re-suspended in 600 µL of $CDCl_3$ and transferred in a 5 mm NMR tube for further 1-D and 2-D NMR analysis. D_2O and $CDCl_3$ were used for locking and shimming.

3 Results and discussions

3.1 Evidence for the formation of oligomers by radical oligomerization of MVK

The aqueous phase OH-oxidation of MVK leads to the formation of series of oligomers as indicated by the analytical devices used, and is in good agreement with the study by Liu et al. (2012). Furthermore, the whole set of analyses showed that the produced oligomers were formed by radical oligomerization of MVK, as discussed below. The ionic oligomerization of MVK (through carbocations or carbanions) was unlikely under our experimental conditions because the protic and nucleophilic characters of the solvent (water) inhibit oligomerization by reacting instantly with carbocation and carbanion initiators (Odian, 2004).

ACPD
13, 2913–2954, 2013

3.1.1 Series of oligomers evidenced by mass spectrometry and NMR spectroscopy

Figure 1 shows a mass spectrum (obtained using UPLC-ESI-MS) for the retention time range 0–7 min, recorded in the positive mode, at 50 min of MVK photooxidation at 5 °C (experiment C in Table 1). Spectra typically contain hundreds of peaks in both modes, and it was out of the scope of this study to explore their full complexity. Yet, oligomer systems are clearly visible, with very regular spacing of 70.0419 Da, which correspond to the exact mass of the precursor, MVK, as confirmed by the ESI-UHRMS analysis. These systems extend up to 1800 Da, thus containing up to 25 monomers. Using a lower intensity xenon lamp, and a lower resolution mass spectrometer (Table 1), Liu et al. (2012) also found oligomer series at the same nominal masses, with slightly different intensities. The main differences observed here were the kinetics. The maximum intensity was reached around 50 min here at 25 °C, instead of 20 h previously (Liu et al., 2012) at the same temperature, certainly due to the higher $HO^{\bullet}$ concentrations obtained here with a more powerful irradiation lamp (Table 1).

Experiment A was repeated 12 times and analyzed using the same UPLC-ESI-MS conditions. The exact masses measured for the oligomers were very repeatable, as was the kinetics of their appearance and of MVK consumption.

Experiment A was also monitored once using ^{1}H NMR spectroscopy (Table 1). Figure 2 shows ^{1}H NMR peaks resonating at 2.36 ppm (s), 6.13 ppm (dd), 6.37 ppm (m) and 6.39 ppm (m) that were assigned to the ^{1}H of MVK. These ^{1}H peaks decreased with time while new ^{1}H NMR signals resonating at 1.15–1.88 ppm and 2.13–2.34 ppm increased with time, indicating the formation of reaction products, to the detriment of MVK. These signals are very wide and are consistent with the presence of overlapping signals due to a variety of oligomers. Overall, both mass spectrometry and NMR measurements indicate that a wide variety of oligomers was formed from the reactivity of MVK and that this formation of high mass oligomers occurs through an extremely fast mechanism, as in radical propagation systems.

ACPD
13, 2913–2954, 2013

3.1.2 Indications on the chemical structure of the monomers according to NMR and UV-spectroscopic measurements

In order to identify the structure of the oligomers observed by ^{1}H NMR spectroscopy in Fig. 2, the sample taken at the end of the reaction (experiment A at 90 min) was freeze-dried and re-suspended in $CDCl_3$ leading to a concentrated solution of the oligomers allowing the measurement of 1-D and 2-D NMR spectra (Fig. 3). The analysis of the ^{1}H NMR resonances in the 1-D ^{1}H NMR spectrum (Fig. 3a) and of the $^{1}J_{1}$H−13C correlations present on the 2D ^{1}H−^{13}C HSQC NMR spectrum (Fig. 3b) allowed proposing assignments of CH, CH_2 and CH_3 functional groups of the putative oligomeric structure shown in Fig. 3. Long range J_{1H-13C} correlations observed on the 2-D ^{1}H−^{13}C HMQC NMR spectrum (Fig. 3c) clearly demonstrated the presence of C=O functional groups belonging to the proposed oligomeric structure. NMR experiments also showed that MVK was largely converted into oligomer forms and that most of the signals of C=C bonds have disappeared at 70 and 90 min of reaction, thus indicating that the oligomers are mostly aliphatic.

Using UV absorption spectroscopy from 190 to 400 nm during experiment A, the evolution of the two intense absorption bands of MVK are shown in Fig. 4. During the photooxidation process, the $n \rightarrow \pi^*$ transition (Fig. 4a) was clearly shifted to shorter wavelengths (blue shift; i.e. from 296 nm at time 0 to 269 nm at 90 min of reaction), with increasing absorption intensity. The $\pi \rightarrow \pi^*$ transition did not show any shift (in the range of the investigated wavelengths) (Fig. 4b), but a clear decrease of its intensity (at 211 nm) was observed. The observed blue shift shows that, in the reaction products formed, the corresponding transition needs higher energy (than in MVK) to get excited (i.e. at shorter wavelengths). This can be due to the loss of the conjugation, probably due to the loss of the vinyl function, in good agreement with the NMR analyses. Furthermore, the absorption intensity at 211 nm was directly proportional to the MVK concentrations during the reaction, as we verified with ^{1}H NMR (at 2.36 ppm) and with mass spectrometry.

ACPD
13, 2913–2954, 2013

3.1.3 Time profiles of MVK, and reaction products

The observed kinetics of the MVK degradation (Fig. 5) were characteristic of those of the monomers in radical polymerization (Pearce et al., 1982). During the initiation step of the reaction (~ 10–15 min at 25 °C), MVK was slowly degraded, and low molecular weight reaction products were formed, such as acetate as observed by 1-D ^{1}H NMR (at 1.90 ppm, Fig. 2). More generally, organic acids were produced, as denoted by the fast decrease of the pH, from 6 to 4, during this step. After ~ 10–15 min, oligomerization started, and the kinetics of MVK degradation significantly increased (Fig. 5). The maximum of oligomers intensity was reached at 50 min of reaction, for the major series. After 90 min of reaction, more than 95 % of MVK was consumed and the oligomers started to decrease.

3.1.4 Comparison of the oligomers formed by OH-oxidation of MVK with a synthetic oligomer of MVK

In order to confirm the radical MVK oligomerization during OH-oxidation, oligomers of MVK were synthesized using a water-soluble radical initiator (V50: 2,2′-Azobis(2-methylpropionamidine) dihydrochloride, Wako) which forms two symmetric radicals by thermal homolysis (Reaction (R6) in Table S2 in the Supplement), under oxygen-free conditions at $T \geq 50$ °C and similar initial concentrations of MVK as in our photooxidation experiments (Table S2 in the Supplement). $[MVK]_0/[V50]_0$ ratio was kept constant at 80 (Table S2 in the Supplement) and UV absorption spectra were monitored at the beginning (t = 0 min) and after the reaction (t = 120 min).

UV absorption spectra obtained during the OH-oxidation of MVK in the aqueous phase (Fig. 4) and after the synthesis of MVK oligomers in the aqueous phase (Fig. S1 in the Supplement) both showed the same blue shift on the $n \rightarrow \pi^*$ transition band (from 296 nm), and a significant decrease of the intensity at 211 nm.

The mass spectra obtained for the synthesized oligomer (Fig. S2 in the Supplement) were very similar to those obtained during the OH-oxidation of MVK in the aqueous

ACPD
13, 2913–2954, 2013

phase (Fig. 1). Figure S2 in the Supplement shows very regular spacing of 70.0419 Da, and a Poisson distribution, typical of polymers (Pearce et al., 1982). Additionally, the method used to identify the initiator radicals (see Sect. 3.2 below), applied to the high resolution mass spectrum obtained from the synthesized oligomers, allowed us to determine the chemical formula of the initiator radical formed from the V50 molecule (Reactions (R6) and (R7) in Table S2 in the Supplement).

Overall, this comparison confirms the radical character of the MVK oligomerization during its OH-oxidation in the aqueous phase under atmospherically relevant conditions.

3.2 Proposed mechanism of radical oligomerization of MVK

In view of the observations performed in Sect. 3.1, we proposed a simple chemical mechanism of radical oligomerization of MVK that is likely to occur during its OH-oxidation in the aqueous phase (Fig. 6). In the initiation step, the reactivity of MVK towards the $HO^{\bullet}$ radical yields (directly or indirectly: see below Sect. 3.4) initiator radicals $iR^{\bullet}$ (Odian, 2004). Each radical adds on another MVK molecule by opening its vinyl double bond, leading to the formation of another radical, $iR–MVK^{\bullet}$ which can then add to another MVK molecule in the same way, and so on, leading to the formation of a large radical, $iR–(MVK)_n–MVK^{\bullet}$. The propagation keeps on increasing the chain length, until the radical termination. Termination occurs by bimolecular reaction between two radicals, by coupling or by disproportionation (Fig. 6), thus yielding, for each initiator radical $iR^{\bullet}$, two oligomer series including one saturated and one unsaturated terminal group (Morton et al., 1973).

This chemical mechanism is in very good agreement with our experimental observations. The regular mass spacing of 70.0419 Da observed in mass spectra (Fig. 1) corresponds exactly to the mass of the monomer MVK in the mechanism. Radical oligomerization is in good agreement with a very fast propagation with prompt growth of the chain to high molecular weight oligomers after an initiation step (Fig. 5). The MVK oligomerization is in good agreement with the significant loss of the vinyl group

ACPD
13, 2913–2954, 2013

observed in Fig. 2 and Fig. 3, which is correlated with a significant loss of double bond conjugation as observed in Fig. 4. Additionally, this is in agreement with the fact that oligomerization of carbon–carbon double bonds is by far more likely than carbonyl groups because of the polarized nature of the latter (Odian, 2004).

Finally, the termination step of the mechanism is in good agreement with the observation of the same degree of polymerization (DP) (i.e. n = number of monomers) for series of oligomers in mass spectra distant by 2.0156 Da (Fig. 1).

The scheme of the proposed mechanism (Fig. 6) only shows external radical additions for clarity. However, both external and internal additions can occur at each step, leading to the formation of a number of isomers that grows exponentially with the DP. This is clearly observed in Fig. S3 in the Supplement showing the extracted UPLC-ESI-MS chromatogram of one of the most intense series of oligomers R–OH–$(MVK)_n$ (S174 colored in red in Fig. 1) formed during OH-oxidation of MVK after 50 min of reaction. The retention time of the oligomers regularly increases with the DP, certainly due to the growth of the corresponding molecules. Additionally, the width of the chromatographic peaks increases with the DP (from n = 1 to n = 5) unambiguously indicating that there are different products at the same mass, probably because of different tacticities of oligomers. After n = 5, the peaks become sharper and their area decreases, indicating that one way of oligomerization may be privileged due to steric hindrance for example. In this series, which is one of the most intense ones, we detected oligomers with a DP up to 23 (n = 23).

3.3 Effects of initial conditions on the oligomer formation

The parameters we varied were chosen for two reasons: (1) for their atmospheric relevance, and (2) because they are known to significantly influence radical polymerization (Odian, 2004). The influence of the initial concentrations of MVK was investigated because the organic concentrations can vary by orders of magnitude in the atmosphere from cloud droplets to deliquesced aerosol particles. The second reason for this choice was to test the influence of initial MVK concentration on the oligomerization process.

ACPD
13, 2913–2954, 2013

Dissolved O_2 is known as a major inhibitor of radical polymerization, and also atmospheric dissolved O_2 concentrations in the condensed phase are not known. Temperature is known to influence not only the kinetics of the reactions but also the oxygen Henry's law equilibrium (Table 1). The results of these experiments allowed us to confirm the mechanism of radical oligomerization of MVK, and also to identify a number of radical initiators (Sect. 3.4).

3.3.1 Effect of initial concentrations of MVK

Between experiments A, E and F (Table 1), initial concentrations of MVK varied from 20 to 0.2 mM with identical temperature (25 °C) and similar initial dissolved O_2 concentration (supersaturated). These three experiments show that different initial concentrations of MVK induced important effects on the oligomer formation, as observed by UPLC-ESI-MS (Fig. 7). The same major series of oligomers were observed at the three initial concentrations, but the chain length increased with the initial MVK concentration. For example, for the series depicted in red color in Fig. 1 and in Fig. 7, the observed DP was 23 at 20 mM initial MVK concentration, 9 at 2 mM, and 4 at 0.2 mM. This correlation between the DP and the initial concentration of MVK is in very good agreement with the kinetic chain length of a radical chain oligomerization (Odian, 2004).

Finally, Fig. 7 clearly shows that for the high initial MVK concentrations (2 and 20 mM), the main reaction products were the oligomers (up to 800 and 1800 Da, respectively), while at the low initial MVK concentration studied (0.2 mM), low molecular weight reaction products were mainly formed (up to 230 Da). It is probable that at the latter initial concentration, we observed the formation of initiators that recombined because the MVK concentration was too low to propagate the radical oligomerization to higher chain lengths.

ACPD
13, 2913–2954, 2013

3.3.2 Effects of initial concentrations of dissolved oxygen and temperature

Experiments A and D (Table 1) were performed under the same initial concentrations of MVK (20 mM) and temperature (25 °C), with very different initial dissolved O_2 concentrations: supersaturated and low initial O_2 concentrations, respectively, i.e. higher and lower than Henry's law equilibrium (by a factor of 1.7 and 4.5, respectively; Table 1). The results showed that the initial dissolved O_2 concentrations had a drastic effect on oligomerization, and on the kinetics of MVK consumption, in very good agreement with a mechanism of radical oligomerization of MVK. Dissolved O_2 is known to inhibit free radical photo-oligomerization by reacting with radical species to form chain terminating oxygenated compounds such as hydroperoxides (Decker and Jenkins, 1985). In our experiments, a clear inhibition of the oligomer formation by dissolved O_2 was observed (Fig. 8a): at low initial O_2 concentrations (experiment D), the whole oligomer series developed within 5 min of reaction, while only first elements of the series appeared at the same reaction time under "supersaturated initial O_2 concentrations" (experiment A). This phenomenon, which was observed for all the other series of oligomers, shows that the reactivity of the initiator radicals ($iR^{\bullet}$) underwent a competition kinetic between their reaction towards O_2 and towards MVK for further oligomerization propagation. When O_2 was present, $iR^{\bullet}$ consumed O_2 very rapidly (i.e. faster than O_2 renewal from the gas phase and from H_2O_2 reactivity), and when O_2 concentration was sufficiently low, the competition furthered the oligomerization pathway which was extremely fast. Figure 9 shows a very contrasting behavior of MVK time profiles between "low initial O_2 concentrations" and "supersaturated initial O_2 concentrations" conditions. Under "supersaturated initial O_2 concentrations", two kinetic steps were observed: a slow one during which the oligomers were poorly formed, followed by a fast one where oligomers were actively formed (Figs. 5 and 9b). In contrast, under "low initial O_2 concentrations", the kinetic of MVK consumption was fast from the beginning (only one step was observed), and oligomerization started as soon as MVK was introduced (Figs. 9a and 8).

ACPD
13, 2913–2954, 2013

Figure 9 also shows the behavior of dissolved O_2 under three different conditions (experiments D, A and C). For all of these conditions, before the injection of H_2O_2, dissolved O_2 was at its Henry's law equilibrium with ambient O_2 in the gas phase. When H_2O_2 was added, dissolved O_2 concentrations increased due to the self-reaction of $HO_2^{\bullet}$ and/or $O_2^{\bullet-}$ radicals in the aqueous phase (see reactions R3 and R4 in the Supplement). Then, as soon as MVK was introduced, the time profiles of O_2 concentration followed those of MVK, thus indicating that O_2 reacted with the radicals formed from MVK, even when oligomerization was the dominant pathway. Interestingly, under "supersaturated initial O_2 concentrations", the oligomerization acceleration started when O_2 concentrations were depleted from their initial values, but still they were higher than their Henry's law equilibrium (by a factor of 1.2 and 1.4 at 25 and 5 °C, respectively), thus showing the atmospheric relevance of these oligomerization processes.

Experiments A, B and C differ for the temperature (i.e., 25 °C, 9 °C and 5 °C) with identical initial concentrations of MVK (20 mM) and similar dissolved O_2 concentration (supersaturated). The kinetic decay of MVK was clearly influenced by the temperature during the initial step (Fig. 9b, c). Additionally, the lower temperature induced higher initial dissolved O_2 concentrations, and both these phenomena explain the time delay of the acceleration of oligomerization at 5 °C compared to 25 °C (at around 25 and 13 min, respectively). In contrast, the fast decay of MVK was not influenced by the temperature, thus showing that the radical mechanism of oligomerization of MVK at 20 mM is the dominant pathway for MVK consumption at this step.

Finally, when most of the MVK was consumed, all oligomer series reached their maximum intensities, with slight differences from one condition to the other as illustrated for one series in Fig. 8b. These differences are particularly interesting to investigate the comprehension of the initial steps of the radical mechanism.

3.4 Identification of oligomers and their initiator radicals

In Fig. 10, starting from the known mechanism of OH-oxidation of MVK in the aqueous phase (Liu, 2011; Zhang et al., 2010), we added the possible oligomerization

ACPD
13, 2913–2954, 2013

developments according to the experimental observations discussed above. The chemical structures of the identified oligomers are shown in Fig. 10 as well as their series names. The latter are also reported in Table 2 together with the corresponding *m/z* and chemical formulas obtained for the first oligomer ($n = 1$) of each series (i.e. iR–$(MVK)_{n=1}$) by UPLC-ESI-MS and ESI-UHRMS analyses. The identification was performed on the smallest oligomer of each series because the resolution and sensitivity of both instruments are optimum for $100 < m/z < 350$ Da. The identifications of the most intense peaks were further confirmed by MS/MS analyses. This method of identification, applied to the synthetic oligomers of MVK formed from the V-50 initiator, allowed us to identify the most intense series of oligomers as the one shown in Reaction (R2) in Supplement 2, thus showing the robustness of the method. The identification of the longer chain oligomers ($n \geq 2$) was further completed by the Kendrick analysis based on the MVK (C_4H_6O) pattern, using the method mentioned in Sect. 2.3.

The oligomers were likely formed according to the mechanism shown in Fig. 6, each one being initiated by an initiator radical $iR^{\bullet}$ formed from the OH-oxidation of MVK (Fig. 10). The OH-oxidation of MVK proceeds via OH-addition (1a) and H-abstraction (1b). For clarity, only external OH-addition is fully developed in Fig. 10, as it is more likely than internal OH-addition, due to steric hindrance. Furthermore, both external and internal OH-additions lead to isomeric forms of oligomers with the same masses which could not be discerned by mass spectrometry. In the proposed mechanism, each step leads to the formation of a radical $iR^{\bullet}$, which undergoes either O_2 addition or oligomerization with MVK, in good agreement with our experimental observations. A detailed description of the mechanism is shown for Pathways 1a and 1b (Fig. 10).

– *Pathway 1a:* OH-addition leads to the formation of radical $R^{\bullet}$, which undergoes either oligomerization with MVK (2a) or O_2 addition (2b). Pathway 2a leads to the formation of radicals $R–(MVK)_n^{\bullet}$ which terminate either directly to form R–$(MVK)_n$ (i.e. series S156 and S158) via the disproportionation mechanism indicated in Fig. 6 or after O_2 addition (3a) followed by H-abstraction (on $HO_2^{\bullet}$, MVK or an oligomer) to form hydroperoxides R–$(MVK)_n$–OOH (series S190) (Decker

ACPD
13, 2913–2954, 2013

and Jenkins, 1985). An isomer of the latter oligomer series (S190) may also be produced from the oligomerization of $ROO^{\bullet}$ radicals, which proceeds via the disproportionation mechanism (Fig. 6). However, this pathway (not shown) is of minor importance because the corresponding unsaturated series (S188) showed a very weak signal by both mass spectrometers (below 1/100 of the most intense series shown in Table 2). $ROO^{\bullet}$ radicals can also undergo self-reaction (4a) leading to a tetroxide which decomposes to form low-molecular-weight compounds (LMWC) oxygenated molecular compounds (as those observed by Zhang et al., 2010) (5c), and $RO^{\bullet}$ radicals (von Sonntag and Schuchmann, 1997) (5a). $ROO^{\bullet}$ radicals can also react with MVK (or $HO_2^{\bullet}$) (4b) to form hydroperoxides ROOH. The latter can be photolyzed (5b) to yield $HO^{\bullet}$ and $RO^{\bullet}$ radicals. These alkoxy radicals undergo either rearrangement (6a) or decomposition (6b). The rearrangement of alkoxy radicals in aqueous medium is a well-known process (Schuchmann and von Sonntag, 1984), it produces (via pathway 6a) more stable radicals $(R{-}OH)^{\bullet}$ which undergo either O_2 reactivity (leading to some of the oxygenated molecular compounds observed by Zhang et al., 2010) or oligomerization with MVK via the disproportionation mechanism (Fig. 6) and form $R{-}OH{-}(MVK)_n$ (series S172, S174). The decomposition (pathway 6b, detailed in Zhang et al., 2010) produces smaller oxygenated compounds, such as methylglyoxal and acetic acid. The latter products react further with $HO^{\bullet}$ radicals to form radicals (as described by Tan et al., 2012) which undergo either O_2 reactivity or oligomerization with MVK via the disproportionation mechanism (Fig. 6) and form series S140′ and S142, and series S128 and S130, respectively.

– *Pathway 1b:* H-abstraction leads to an unsaturated radical, $MVK^{\bullet}$, which can also be formed via pathway (4b), as mentioned above. $MVK^{\bullet}$ radicals undergo either oligomerization with MVK via the disproportionation mechanism (Fig. 6) and terminate (7a) into $(MVK){-}(MVK)_n$ (series S138 and S140) or O_2 addition (7b) and further react to produce $MVK{-}OH{-}(MVK)_n$ (series S154 and S156′).

ACPD
13, 2913–2954, 2013

In this mechanism, the formed low-molecular-weight compounds (LMWC, such as formaldehyde, methylglyoxal, glyoxal, oxalic, formic, pyruvic, malonic and acetic acids, observed by Zhang et al., 2010 during the OH-oxidation of MVK under similar conditions) can also further react with $HO^{\bullet}$ and produce other $iR^{\bullet}$ radicals, which can oligomerize. However, the corresponding oligomers were observed here only for acetic acid and methylglyoxal, which were among the major low-molecular-weight products observed by Zhang et al. (2010). A confirmation of these observations was brought by two extra experiments (A′ and A″) where 2 mM of methylglyoxal and acetic acid (Sigma Aldrich), respectively, were injected in the vessel at the same time as MVK injection. The results showed a significant increase (by 42 % and 77 %, respectively) of the corresponding oligomer series (S140′ and S142 and series S128 and S130, respectively), compared to experiment A. Furthermore, experiment C (performed at 5 °C) allowed us to clearly observe the kinetics of oligomer formation (Fig. 11). The series R–$(MVK)_n$ (S156) were directly formed, immediately followed by the series R–$(MVK)_n$–OOH (S190) (which require O_2 addition), and the series (Methylglyoxal)–$(MVK)_n$ (S142) and (Acetic acid)–$(MVK)_n$ (S130) were formed later, in very good agreement with the proposed mechanism (in Fig. 10).

The role of molecular O_2 was evidenced by the intensities of the identified series (Table 2). Comparing experiments A and D (i.e. from supersaturated to low initial O_2 conditions, respectively), after 50 min of reaction, we observed a systematic increase of the intensities of all series not requiring O_2 addition, and a systematic decrease of those requiring O_2 addition. This observation is also in very good agreement with the proposed mechanism (Fig. 10) described above, and it shows the prevailing role of oxygen on the processes.

4 Conclusions

This paper reports on an experimental study of the aqueous phase OH-oxidation of methyl vinyl ketone, under atmospheric conditions of clouds or deliquesced aerosol

ACPD
13, 2913–2954, 2013

particles. In good agreement with Liu et al. (2012), we showed that this reactivity leads to the formation of oligomers via a radical oligomerization mechanism. Using mass spectrometry, 26 series of oligomers were detected with highly regular patterns of mass differences of 70.0419 Da (corresponding to the molecular mass of MVK) up to 1800 Da, in both positive and negative modes. Additionally, the kinetics of the reactions, monitored by NMR and UV spectroscopy, indicated that MVK was largely converted into oligomeric forms with the decrease of the olefin structures, correlated with the increase of aliphatic carbonyl oligomers. Using high and ultra-high resolution mass spectrometry, the elemental composition of 13 series of oligomers was determined.

The investigation of the influence of key parameters, i.e. temperature, initial MVK concentrations and initial dissolved O_2 concentrations showed important impacts on the oligomerization process. The mass of oligomers increased with the initial MVK concentrations. Under supersaturated initial O_2 concentrations, the initiation of oligomerization was delayed compared to low initial O_2 concentrations, and this delay increased with decreasing temperature.

In agreement with the experimental observations, we proposed a complete radical mechanism of OH-oxidation of MVK in the aqueous phase proceeding via oligomerization of MVK by opening its carbon-carbon double bond, initiated from several initiator organic radicals ($iR^{\bullet}$). Among the latter were those directly formed by OH-oxidation of MVK, and also those formed from the OH-oxidation of MVK's main oxidation products, e.g. acetic acid and methylglyoxal. The proposed mechanism allowed for explaining the particular role of dissolved O_2 under our experimental conditions. Each $iR^{\bullet}$ radical underwent competition kinetics between O_2 addition (Reaction R1) and oligomerization (Reaction R2):

$$iR^{\bullet} + O_2 \rightarrow \text{LMWC} \quad \text{(R1)}$$

$$iR^{\bullet} + n(\text{MVK}) \rightarrow \text{oligomers} \quad \text{(R2)}$$

Supersaturated initial O_2 concentrations inhibited radical oligomerization by fast addition on $iR^{\bullet}$ resulting in the formation of LMWC (such as acetic acid and methylglyoxal),

ACPD
13, 2913–2954, 2013

which were further OH-oxidized and formed other $iR^{\bullet}$ radicals. The fast O_2 addition reactions resulted in a fast decrease of O_2 concentrations in the vessel, faster than O_2 renewal from the gas phase and from the reactivity of H_2O_2, and even faster than MVK consumption. At initial MVK concentrations higher than 0.2 mM, the decrease of O_2 concentrations resulted in the dominance of reaction (2) after several minutes, and oligomerization started, even when O_2 concentrations were still higher than Henry's law equilibrium with atmospheric O_2. The paradoxical role of O_2 resides in the fact that while it inhibits oligomerization, it produces more $iR^{\bullet}$ radicals, which contribute to O_2 consumption, and thus lead to oligomerization. These processes, together with the large ranges of initial concentrations investigated (60–656 µM of dissolved O_2 and 0.2–20 mM of MVK concentrations) show the fundamental role that O_2 likely plays in atmospheric aerosols. Further studies are needed to investigate the actual ranges of O_2 concentrations in the condensed phases in order to assert the importance of the oligomerization processes established here in the atmosphere.

In the proposed mechanism, some ubiquitous radicals in the atmospheric aqueous phase (such as those resulting from the reactivity of acetic acid and methylglyoxal) can be very efficient initiator radicals. The latter radicals simply require sufficiently concentrated olefins to initiate oligomerization with fast propagation and prompt growth of the chain, resulting in the formation of very high molecular weight compounds. It is thus of high interest to investigate the potential concentrations of olefin structures in the condensed phase of the atmosphere.

In the proposed mechanism, oligomerization mechanisms proceed via non-oxidative pathways. Such pathways in the aqueous phase can explain some atmospheric observations such as those of Mazzoleni et al. (2012) who investigated elemental composition of WSOC by ultra-high resolution mass spectrometry. Their results indicated significant non-oxidative reaction pathways for the formation of high molecular weight WSOC components in organic aerosols sampled during summer in a rural site where SOA was abundant.

ACPD
13, 2913–2954, 2013

Supplementary material related to this article is available online at: http://www.atmos-chem-phys-discuss.net/13/2913/2013/acpd-13-2913-2013-supplement.pdf.

Acknowledgements. We thank the National Research Agency ANR (project Cumulus), AXA insurances and CNRS-INSU for funding this research. We also thank Barbara Ervens (CIRES, University of Colorado, Boulder and Chemical Sciences Division, National Oceanic and Atmospheric Administration (NOAA), Boulder, CO, USA) and Gaëlle Gosset (Aix-Marseille Université, CNRS, ICR UMR 7273, 13397, Marseille, France) for valuable scientific discussions on this topic.

References

Bateman, A. P., Walser, M. L., Desyaterik, Y., Laskin, J., Laskin, A., and Nizkorodov, S. A.: The effect of solvent on the analysis of secondary organic aerosol using electrospray ionization mass spectrometry, Environ. Sci. Technol., 42, 7341–7346, doi:10.1021/es801226w, 2008.

Benson, B. B. and Krause, D.: The concentration and isotopic fractionation of oxygen dissolved in freshwater and seawater in equilibrium with the atmosphere, American Society of Limnology and Oceanography Inc., Department of Physics, Amherst College, Amherst, Massachusetts, USA, 1984.

Carlton, A. G., Wiedinmyer, C., and Kroll, J. H.: A review of Secondary Organic Aerosol (SOA) formation from isoprene, Atmos. Chem. Phys., 9, 4987–5005, doi:10.5194/acp-9-4987-2009, 2009.

Danger, G., Orthaus-Daunay, F. R., de Marcellus, P., Modica, P., Vuitton, V., Duvernay, F., Flandinet, L., Le Sergeant d'Hendecourt, L., Thissen, R., and Chiavassa, T.: Characterization of laboratory analogs of interstellar/cometary organic residues using very high resolution mass spectrometry, Geochim. Cosmochim. Acta, submitted, 2013.

Decesari, S., Facchini, M. C., Fuzzi, S., McFiggans, G. B., Coe, H., and Bower, K. N.: The water-soluble organic component of size-segregated aerosol, cloud water and wet depositions from Jeju Island during ACE-Asia, Atmos. Environ., 39, 211–222, 2005.

ACPD
13, 2913–2954, 2013

Decker, C. and Jenkins A. D.: Kinetic approach of O_2 inhibition in ultraviolet- and laser-induced polymerizations, Macromolecules, 18, 1241, doi: 10.1021/ma00148a034, 1985.
Ervens, B. and Volkamer, R.: Glyoxal processing by aerosol multiphase chemistry: towards a kinetic modeling framework of secondary organic aerosol formation in aqueous particles, Atmos. Chem. Phys., 10, 8219–8244, doi:10.5194/acp-10-8219-2010, 2010.
Ervens, B., Turpin, B. J., and Weber, R. J.: Secondary organic aerosol formation in cloud droplets and aqueous particles (aqSOA): a review of laboratory, field and model studies, Atmos. Chem. Phys., 11, 11069–11102, doi:10.5194/acp-11-11069-2011, 2011.
Gibian, M. J. and Corley, R. C.: Organic radical-radical reactions. Disproportionation vs. combination, Chem. Rev., 73, 441–464, doi:10.1021/cr60285a002, 1973.
Hallquist, M., Wenger, J. C., Baltensperger, U., Rudich, Y., Simpson, D., Claeys, M., Dommen, J., Donahue, N. M., George, C., Goldstein, A. H., Hamilton, J. F., Herrmann, H., Hoffmann, T., Iinuma, Y., Jang, M., Jenkin, M. E., Jimenez, J. L., Kiendler-Scharr, A., Maenhaut, W., McFiggans, G., Mentel, Th. F., Monod, A., Prévôt, A. S. H., Seinfeld, J. H., Surratt, J. D., Szmigielski, R., and Wildt, J.: The formation, properties and impact of secondary organic aerosol: current and emerging issues, Atmos. Chem. Phys., 9, 5155–5236, doi:10.5194/acp-9-5155-2009, 2009.
Hennigan, C. J., Bergin, M. H., Russell, A. G., Nenes, A., and Weber, R. J.: Gas/particle partitioning of water-soluble organic aerosol in Atlanta, Atmos. Chem. Phys., 9, 3613–3628, doi:10.5194/acp-9-3613-2009, 2009.
Herrmann, H., Hoffmann, D., Schaefer, T., Bräuer, P., and Tilgner, A.: Tropospheric aqueous phase free radical chemistry: radical sources, spectra, reaction kinetics and prediction tools, Chem. Phys. Phys. Chem., 11, 3796–3822, 2010.
Hobby, K.: A novel method of isotope prediction applied to elemental composition analysis, Micromass MS Technologies, Floats Road, Manchester, M23 9LZ, UK, Waters Corporation, 2005.
Huang, D., Zhang, X., Chen, Z. M., Zhao, Y., and Shen, X. L.: The kinetics and mechanism of an aqueous phase isoprene reaction with hydroxyl radical, Atmos. Chem. Phys., 11, 7399–7415, doi:10.5194/acp-11-7399-2011, 2011.
Hughey, C. A., Hendrickson, C. L., Rodgers, R. P., and Marshall, A. G.: Kendrick mass defect spectrum: a compact visual analysis for ultrahigh-resolution broadband mass spectra, Anal. Chem., 73, 4676–4681, 2001.

ACPD
13, 2913–2954, 2013

Iraci, L. T., Baker, B. M., Tyndall, G. S., and Orlando, J. J.: Measurements of the Henry's law coefficients of 2-methyl-3-buten-2-ol, methacrolein, and methyl vinyl ketone, J. Atmos. Chem., 33, 321–330, 1999.
Li, Y. and Schellhorn, H. E.: Rapid kinetic microassay for catalase activity, J. Biomol. Tech., 18, 185–187, 2007.
Lim, Y. B., Tan, Y., Perri, M. J., Seitzinger, S. P., and Turpin, B. J.: Aqueous chemistry and its role in secondary organic aerosol (SOA) formation, Atmos. Chem. Phys., 10, 10521–10539, doi:10.5194/acp-10-10521-2010, 2010.
Liu, Y.: Etudes des impacts de la réactivité en phase aqueuse atmosphérique sur la formation et le vieillissement des Aérosols Organiques Secondaires sous conditions simulées, Ph. D. thesis, Laboratoire de Chimie de l'Environnement, Aix-Marseille University, Marseille, France, 2011.
Liu, Y., El Haddad, I., Scarfogliero, M., Nieto-Gligorovski, L., Temime-Roussel, B., Quivet, E., Marchand, N., Picquet-Varrault, B., and Monod, A.: In-cloud processes of methacrolein under simulated conditions – Part 1: Aqueous phase photooxidation, Atmos. Chem. Phys., 9, 5093–5105, doi:10.5194/acp-9-5093-2009, 2009.
Liu, Y., Siekmann, F., Renard, P., El Zein, A., Salque, G., El Haddad, I., Temime-Roussel, B., Voisin, D., Thissen, R., and Monod, A.: Oligomer and SOA formation through aqueous phase photooxidation of methacrolein and methyl vinyl ketone, Atmos. Environ., 49, 123–129, doi:10.1016/j.atmosenv.2011.12.012, 2012.
Makarov, A., Denisov, E., Lange, O. and Horning, S.: Dynamic range of mass accuracy in LTQ orbitrap hybrid mass spectrometer, J. Am. Soc. Mass Spectr., 17, 977–982, doi:10.1016/j.jasms.2006.03.006, 2006.
Mazzoleni, L. R., Saranjampour, P., Dalbec, M. M., Samburova, V., Hallar, A. G., Zielinska, B., Lowenthal, D. H., and Kohl, S.: Identification of water-soluble organic carbon in non-urban aerosols using ultrahigh-resolution FT-ICR mass spectrometry: organic anions, Environ. Chem., 9, 285–297, doi:10.1071/EN11167, 2012.
Odian, G.: Principles of Polymerization, John Wiley & Sons, Hoboken, New Jersey, 2004.
Orthous-Daunay, F. R.: Empreinte moléculaire des processus post-accrétionnels dans la matière organique des chondrites carbonées, Ph. D. thesis, Institut de Planetelogie et d'Astrophysique, Université Joseph Fourier, Grenoble, France, 2011.

ACPD
13, 2913–2954, 2013

Pearce, E. M., Wright, C. E., and Bordoloi, B. K.: Laboratory Experiments in Polymer Synthesis and Characterization, Educational Modules for Materials Science and Engineering Project, Elsevier, USA, 1–22, 1982.

Schuchmann, H.-P. and von Sonntag, C.: Methylperoxyl radicals: a study of the γ-radiolysis of methane in oxygenated aqueous solutions, Z. Naturforsch. B, 39, 217–221, 1984.

Tan, Y., Carlton, A. G., Seitzinger, S. P., and Turpin, B. J.: SOA from methylglyoxal in clouds and wet aerosols: measurement and prediction of key products, Atmos. Environ., 44, 5218–5226, 2010.

Tan, Y., Lim, Y. B., Altieri, K. E., Seitzinger, S. P., and Turpin, B. J.: Mechanisms leading to oligomers and SOA through aqueous photooxidation: insights from OH radical oxidation of acetic acid and methylglyoxal, Atmos. Chem. Phys., 12, 801–813, doi:10.5194/acp-12-801-2012, 2012.

von Sonntag, C. and Schuchmann, H.-P.: Peroxyl radicals in aqueous solution, In: Peroxyl Radicals, edited by: Alfassi, Z. B., Wiley, Chichester, pp. 173–234, 1997.

Yadav, L. D. S.: Organic Spectroscopy, Kluwer Academic, Secaucus, NJ, U.S.A., 7–51, 2012.

Zhang, X., Chen, Z. M., and Zhao, Y.: Laboratory simulation for the aqueous OH-oxidation of methyl vinyl ketone and methacrolein: significance to the in-cloud SOA production, Atmos. Chem. Phys., 10, 9551–9561, doi:10.5194/acp-10-9551-2010, 2010.

ACPD

13, 2913–2954, 2013

Table 1. Experimental conditions of OH-oxidation of MVK, and comparison with our previous work, the study by Liu et al. (2012). In all studies, all experiments were unbuffered (free pH).

Exp. name/ Ref.	$[MKV]_0$ (mM)	$[H_2O_2]_0$ (mM)	O_2 conditions ($[O_2]_0$ µM)[a, b]	$[O_2]$ (µM) at Henry's Law equilibrium[c]	Temp. (°C)	Lamp (W)	J (s^{-1})	$[HO^\bullet]$[d] (M)	τ_{life} (min)[e]	Analysis (number of experimental repetitions)
Liu et al., 2012	20	1000	Supersaturated (1700)[a]	258	25	300	7.5×10^{-7}	8.6×10^{-15}	262	HPLC-ESI-MS
A	20	400	Supersaturated (400)[a]	258	25	1000	8.5×10^{-6}	4.3×10^{-14}	52	UPLC-ESI-MS (12) ESI-UHRMS (1) UV-spectroscopy (3) NMR-spectroscopy (1)
B	20	400	Supersaturated (580)[a]	361	9	1000	8.5×10^{-6}	4.3×10^{-14}	52	UPLC-ESI-MS (1)
C	20	400	Supersaturated (656)[a]	399	5	1000	8.5×10^{-6}	4.3×10^{-14}	52	UPLC-ESI-MS (4)
D	20	400	Low (60)[b]	258	25	1000	8.5×10^{-6}	4.3×10^{-14}	52	UPLC-ESI-MS (4)
E	2	40	Supersaturated (320)[a]	258	25	1000	8.5×10^{-6}	4.3×10^{-14}	52	UPLC-ESI-MS (2) UV-spectroscopy (1)
F	0.2	4	Supersaturated (280)[a]	258	25	1000	8.5×10^{-6}	4.3×10^{-14}	52	UPLC-ESI-MS (2) UV-spectroscopy (1)

[a] Dissolved O_2 concentration at time 0 (i.e. MVK introduction), in presence of H_2O_2, surrounded by ambient air; [b] dissolved O_2 concentration at time 0, in presence of H_2O_2, after 30 min of argon flow bubbling into the solution; [c] theoretical $[O_2]$ (µM) at Henry's Law equilibrium in ambient air before H_2O_2 addition from Benson and Krause (1984); [d] the $HO^\bullet$ concentrations were calculated assuming the steady state approximation at time 0: $[OH] = \frac{2 \times J \times [H_2O_2]}{k_{MVK} \times [MVK] + k_2 \times [H_2O_2]}$; [e] MVK life time towards OH-oxidation: $\tau_{life} = \frac{1}{k_{MVK}[OH]}$.

ACPD
13, 2913–2954, 2013

Table 2. Oligomer series identified by UPLC-ESI-MS and ESI-UHRMS in positive and negative modes.

Name[a]	Series Formulas[b]	iR-(MVK)$_{n=1}$ Formulas[c]	*m/z* (Da)[c]	$\Delta^{d}_{intensity}$
S138	MVK–(MVK)$_n$	$[C_8H_{10}O_2, +H]^+$	139.0759	+13 %
S140		$[C_8H_{12}O_2, +H]^+$	141.0916	+30 %
S156	R–(MVK)$_n$	$[C_8H_{12}O_3, +H]^+$	157.0865	+12 %
S158		$[C_8H_{14}O_3, +Na]^+$	181.0841	+10 %
S154	MVK–OH–(MVK)$_n$	$[C_8H_{10}O_3, -H]^-$	153.0552	−19 %
S156′		$[C_8H_{12}O_3, -H]^-$	155.0708	−6 %
S190	R–(MVK)$_n$–OOH	$[C_8H_{14}O_5, +Na]^+$	213.0739	−6 %
S172	R–OH–(MVK)$_n$	$[C_8H_{12}O_4, -H]^-$	171.0657	−16 %
S174		$[C_8H_{14}O_4, +Na]^+$	197.0814	−2 %
S128	(Acetic acid)–(MVK)$_n$	$[C_6H_8O_3, -H]^-$	127.0395	−39 %
S130		$[C_6H_{10}O_3, -H]^-$	129.0552	−17 %
S140′	(Methylglyoxal)–(MVK)$_n$	$[C_7H_8O_3, -H]^-$	139.0395	−28 %
S142		$[C_7H_{10}O_3, -H]^-$	141.0552	−12 %

[a] For each series, the name is given by "S" followed by a number corresponding to the nominal mass of the first oligomer, i.e. iR–(MVK)$_{n=1}$. [b] The chemical structures are given in Fig. 10. R$^\bullet$ corresponds to the radical:  [c] Ions (and corresponding *m/z*) identified by UPLC-ESI-MS and/or ESI-UHRMS in experiment A; [d] Intensity ratio of the series after 50 min of OH-oxidation of MVK (20 mM): $\Delta_{intensity} = \frac{TSI_{LowO_2} - TSI_{supersaturatedO_2}}{TSI_{supersaturatedO_2}}$, with: TSI = total Series' intensity.

ACPD
13, 2913–2954, 2013

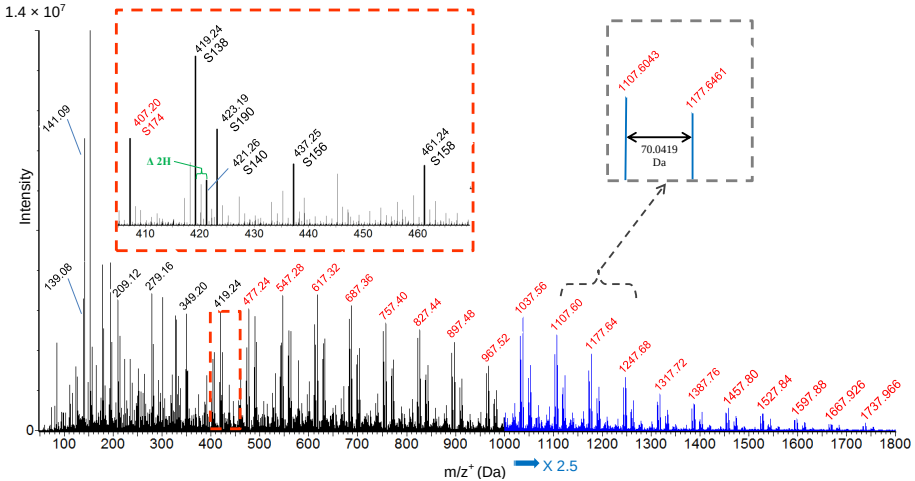

Fig. 1. Mass spectrum (obtained using UPLC-ESI-MS from 0 to 1800 Da) for the retention time range 0–7 min, in the positive mode, at t = 50 min of experiment C. The most intense series (S174) is highlighted in red. Each group of peaks represents a Degree of Polymerization (DP). Left zoom: main series detected for DP = 4. Right zoom: MVK regular pattern of mass differences of 70.0419 Da. Another regular pattern of mass difference of 2.0157 Da corresponding to 2 H is also observed (in green in the left zoom).

ACPD
13, 2913–2954, 2013

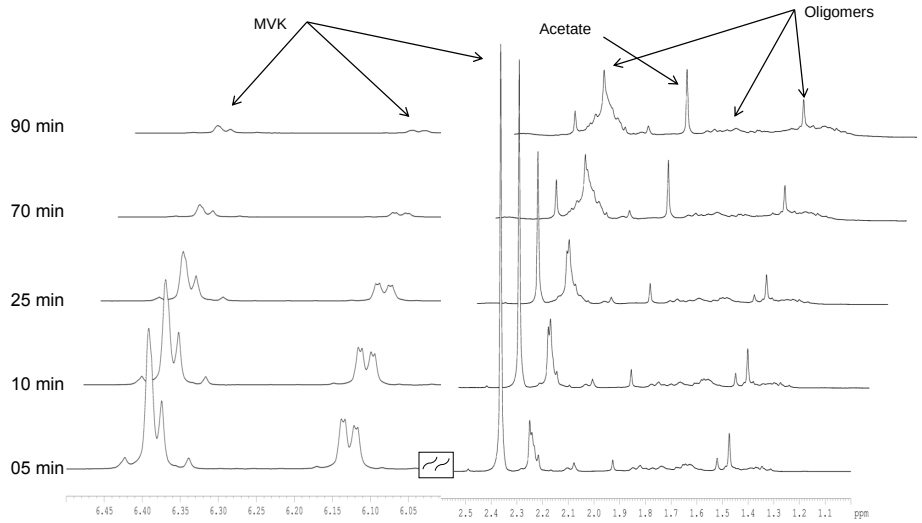

Fig. 2. Monitoring experiment A by 1-D ^{1}H NMR (recorded in phosphate buffer containing 10 % D_2O). The intensities of oligomer structures increase with time, to the detriment of MVK.

ACPD
13, 2913–2954, 2013

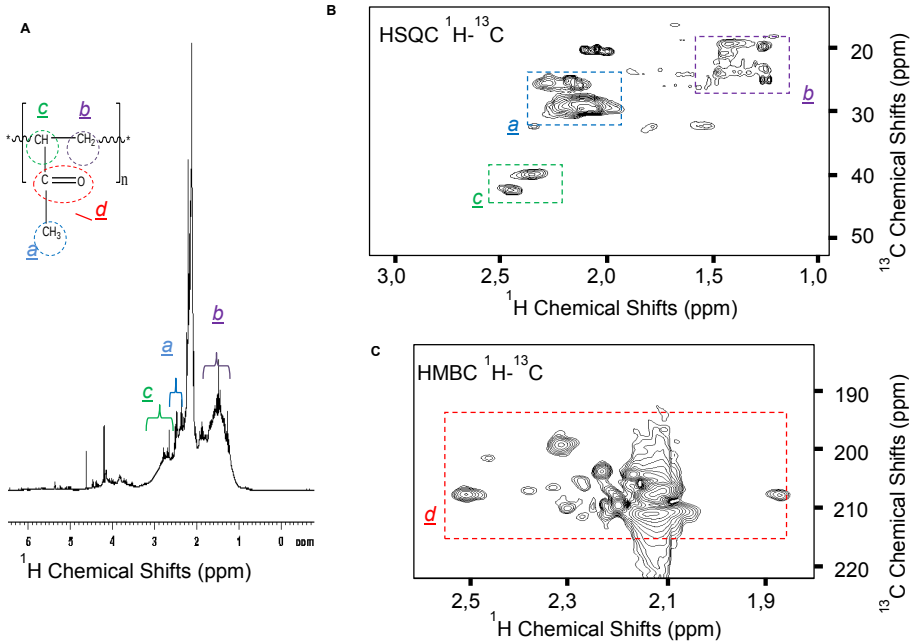

Fig. 3. Proposed structure identification of oligomers. 1-D ^{1}H NMR spectrum **(A)** and 2-D ^{1}H–^{13}C NMR spectra (**B** and **C**) of a sample taken at 90 min of reaction during experiment A, freeze-dried and re-suspended in $CDCl_3$.

ACPD
13, 2913–2954, 2013

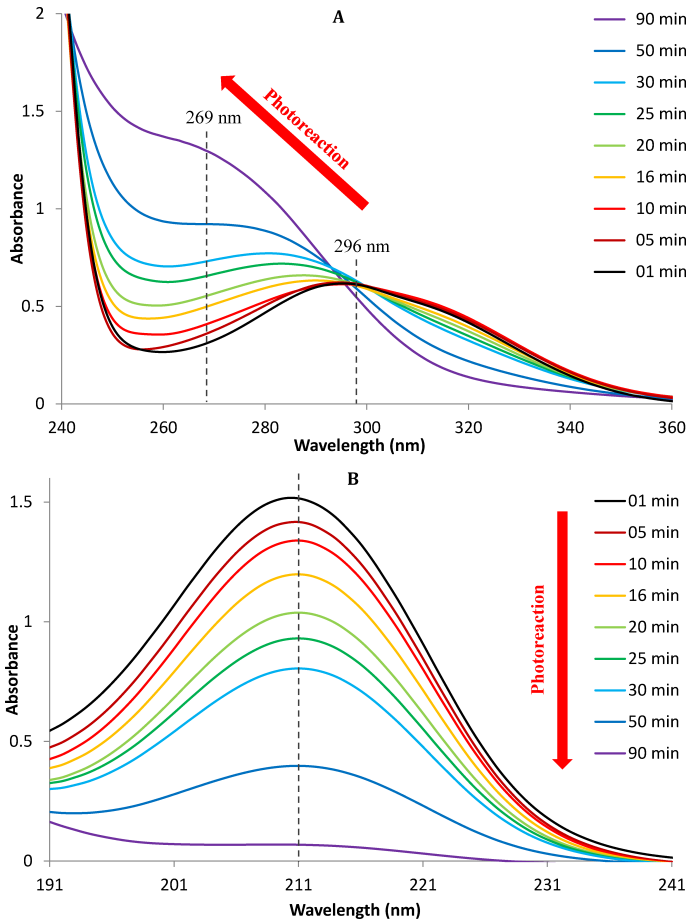

Fig. 4. UV absorption spectra of the solutions sampled during experiment A (with catalase added prior to analysis), **(A)**: from 240 to 360 nm; and **(B)**: diluted by 100 from 191 to 241 nm.

ACPD
13, 2913–2954, 2013

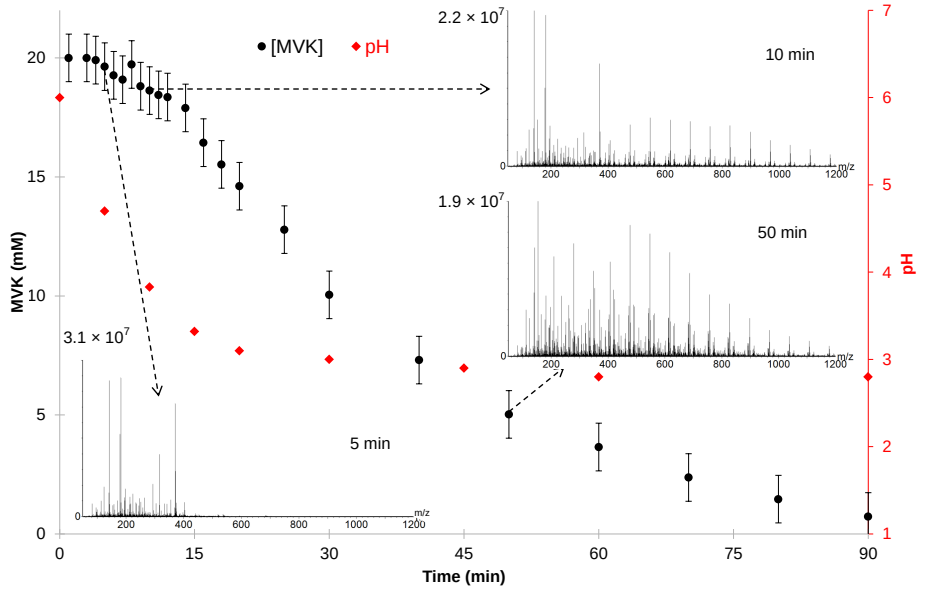

Fig. 5. MVK time profile (as measured by UV Spectroscopy) and mass spectra (obtained using UPLC-ESI-MS for the retention time range 0–5 min in the positive mode) at 5, 10 and 50 min of reaction, during experiment A (MVK 20 mM, 25 °C, under supersaturated O_2 initial conditions).

ACPD
13, 2913–2954, 2013

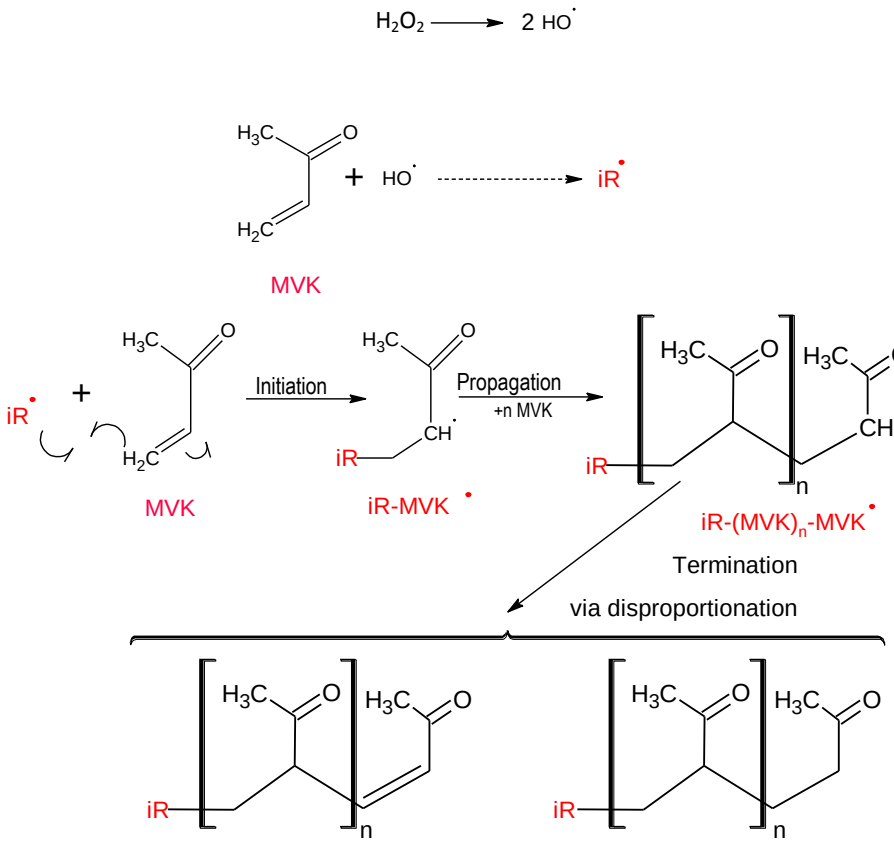

Fig. 6. Scheme of the proposed mechanism of radical oligomerization of MVK in the aqueous phase, initiated by OH-oxidation. iR• is an initiator Radical; MVK is the monomer or the repeating unit, *n* is the degree of polymerization. For clarity, only the external radical additions are shown.

ACPD
13, 2913–2954, 2013

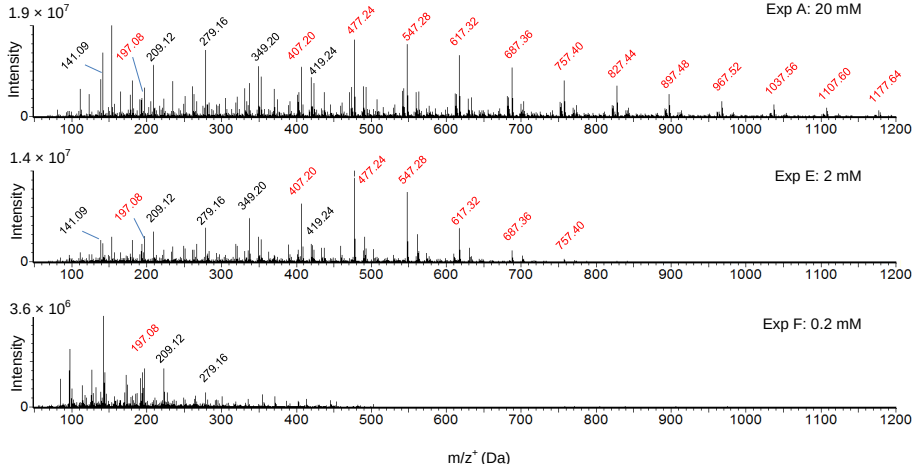

Fig. 7. Mass spectra (obtained using UPLC-ESI-MS, for the retention time range 0–5 min, in the positive mode) during experiments A, E and F (i.e. at 25 °C, for different initial MVK concentrations and at different reaction times (corresponding to the maximum oligomers intensity): 5 min for 0.2 mM; 15 min for 2 mM and 50 min for 20 mM. The most intense series (S174) is highlighted in red, as in Fig. 1).

ACPD
13, 2913–2954, 2013

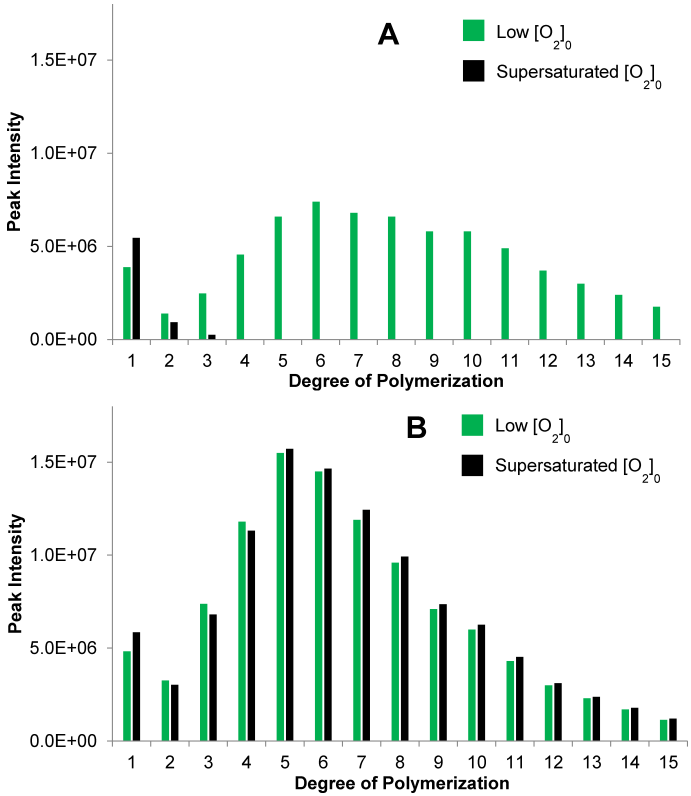

Fig. 8. Effect of initial O_2 concentrations on the oligomer series S174 up to 1200 Da (obtained using UPLC-ESI-MS, for the retention time range 0–5 min, in the positive mode) after **(A)** 5 min and **(B)** 50 min of OH-oxidation of MVK in the aqueous phase at 25 °C, under initial low O_2 conditions (in green: $[O_2]_0$=60 µM), and under initial supersaturated O_2 conditions (in black: $[O_2]_0$=400 µM).

ACPD
13, 2913–2954, 2013

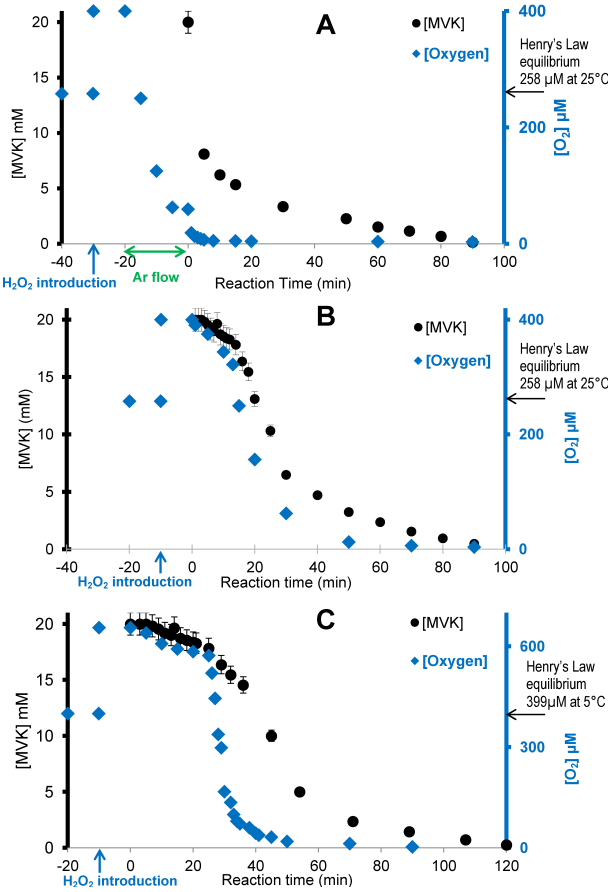

Fig. 9. Time profile of MVK and dissolved O_2 concentrations under different temperature and initial O_2 concentrations: **(A)** experiment D (25 °C, under low initial O_2 concentration: 60 µM); **(B)** experiment A (25 °C, under supersaturated initial O_2 concentration: 400 µM); **(C)** experiment C (5 °C, under supersaturated initial O_2 concentration: 400 µM). Time 0 = MVK introduction.

ACPD
13, 2913–2954, 2013

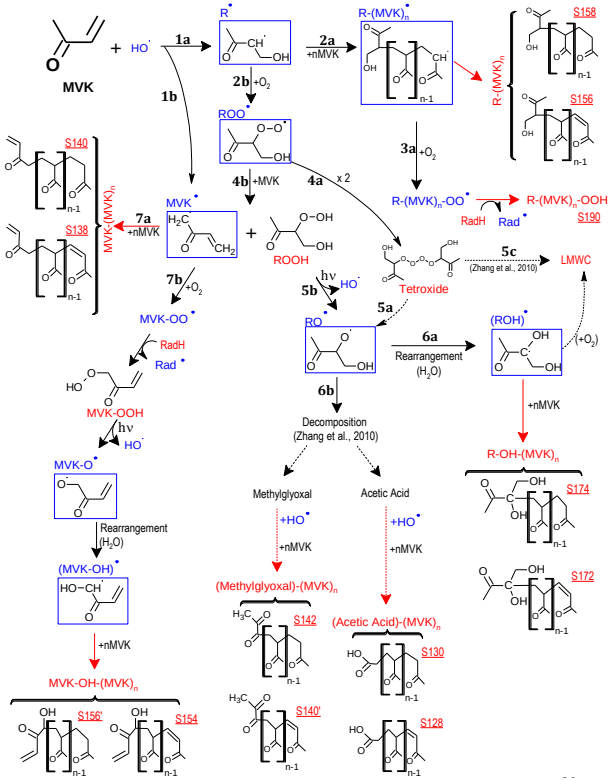

Fig. 10. Proposed scheme of the chemical mechanism of OH-oxidation of MVK in the aqueous phase with implementation of radical oligomerization pathways (for clarity, only external OH-addition on MVK is developed). RadH = MVK, $HO_2^{\bullet}$ or molecular reaction products (in red). Radicals (in blue). LMWC: low-molecular-weight compounds.

ACPD
13, 2913–2954, 2013

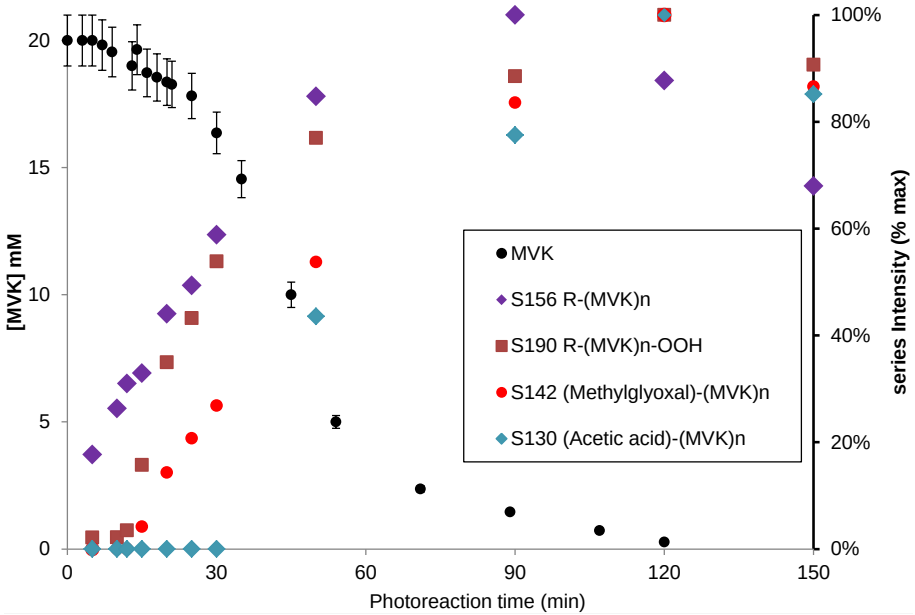

Fig. 11. MVK kinetics and Time profile of main oligomers series (obtained using UPLC-ESI-MS, for the retention time range 0–7 min, in both modes) at 5 °C. The series intensity is the sum of the peaks intensity. Each series intensity is expressed as a percentage of its maximum.

ACPD
13, 2913–2954, 2013